Seasonal evolution of the albedo of multiyear Arctic sea ice

D. K. Perovich

Engineer Research and Development Center, Cold Regional Research and Engineering Laboratory, Hanover, New Hampshire, USA

T. C. Grenfell, B. Light, and P. V. Hobbs

Department of Atmospheric Sciences, University of Washington, Seattle, Washington, USA

Received 16 May 2000; revised 15 January 2001; accepted 23 July 2001; published 11 October 2002.

[1] As part of ice albedo feedback studies during the Surface Heat Budget of the Arctic Ocean (SHEBA) field experiment, we measured spectral and wavelength-integrated albedo on multiyear sea ice. Measurements were made every 2.5 m along a 200-m survey line from April through October. Initially, this line was completely snow covered, but as the melt season progressed, it became a mixture of bare ice and melt ponds. Observed changes in albedo were a combination of a gradual evolution due to seasonal transitions and abrupt shifts resulting from synoptic weather events. There were five distinct phases in the evolution of albedo: dry snow, melting snow, pond formation, pond evolution, and fall freeze-up. In April the surface albedo was high (0.8–0.9) and spatially uniform. By the end of July the average albedo along the line was 0.4, and there was significant spatial variability, with values ranging from 0.1 for deep, dark ponds to 0.65 for bare, white ice. There was good agreement between surface-based albedos and measurements made from the University of Washington's Convair-580 research aircraft. A comparison between net solar irradiance computed using observed albedos and a simplified model of seasonal evolution shows good agreement as long as the timing of the transitions is accurately determined. *INDEX TERMS:* 4540 Oceanography: Physical: Ice mechanics and air/sea/ice exchange processes; 4552 Oceanography: Physical: Ocean optics; 4207 Oceanography: General: Arctic and Antarctic oceanography; *KEYWORDS:* sea ice, albedo, ice-albedo feedback

Citation: Perovich, D. K., T. C. Grenfell, B. Light, and P. V. Hobbs, Seasonal evolution of the albedo of multiyear Arctic sea ice, *J. Geophys. Res.*, *107*(C10), 8044, doi:10.1029/2000JC000438, 2002.

1. Introduction

[2] The ice albedo feedback mechanism plays a key role in the heat and mass balance of the ice and upper ocean in the Arctic [*Maykut and Untersteiner*, 1971; *Curry et al.*, 1995]. During the summer melt season, the sea ice cover undergoes profound changes in its physical state and optical properties. As incident solar radiation increases and the air warms, the ice cover evolves from a highly scattering, snow-covered medium to a darker combination of bare ice, melt ponds and leads (Figure 1). Summer melt rates as well as the duration of the melt season are strongly influenced by the albedo, which decreases as the melt season progresses.

[3] An improved, quantitative understanding of the ice albedo feedback is needed to better model the role of the Arctic sea ice cover in global warming [*Spelman and Manabe*, 1984; *Dickinson et al.*, 1987; *Washington and Meehl*, 1986; *Ingram et al.*, 1989]. To achieve this, it is necessary to determine how shortwave radiation is distributed within the ice-ocean system, and how this distribution affects heat and mass exchange within the system.

0148-0227/02/2000JC000438$09.00

[4] This would be a much simpler task if the ice cover were uniform and homogeneous; a time series of observations at a single point would suffice. However, the summer ice cover is far from uniform, with surface conditions varying from deep snow to bare ice to melt ponds to open leads, and with ice thickness ranging from zero (open water) to ridges tens of meters thick, all within an area that is often less than one square kilometer. Each of these categories has a significantly different set of physical and optical properties, and each processes the incoming shortwave energy differently. To determine how average albedo changes within a large area (e.g., a general circulation model grid cell), we must examine both the temporal and spatial variability of albedo in each of these ice categories and monitor seasonal changes in the fractional area occupied by these categories.

[5] There is an ample database defining wavelength-integrated and spectral albedos for a wide variety of ice types and conditions [*Langleben*, 1969, 1971; *Grenfell and Maykut*, 1977; *Grenfell and Perovich*, 1984; *Buckley and Trodahl*, 1987; *Perovich*, 1991, 1994, 1996; *Perovich et al.*, 1998; *Radionov et al.*, 1997]. These studies have demonstrated the considerable variability of albedo and have established a strong dependence of albedo on surface conditions and the structure of the upper 30–50 cm of the

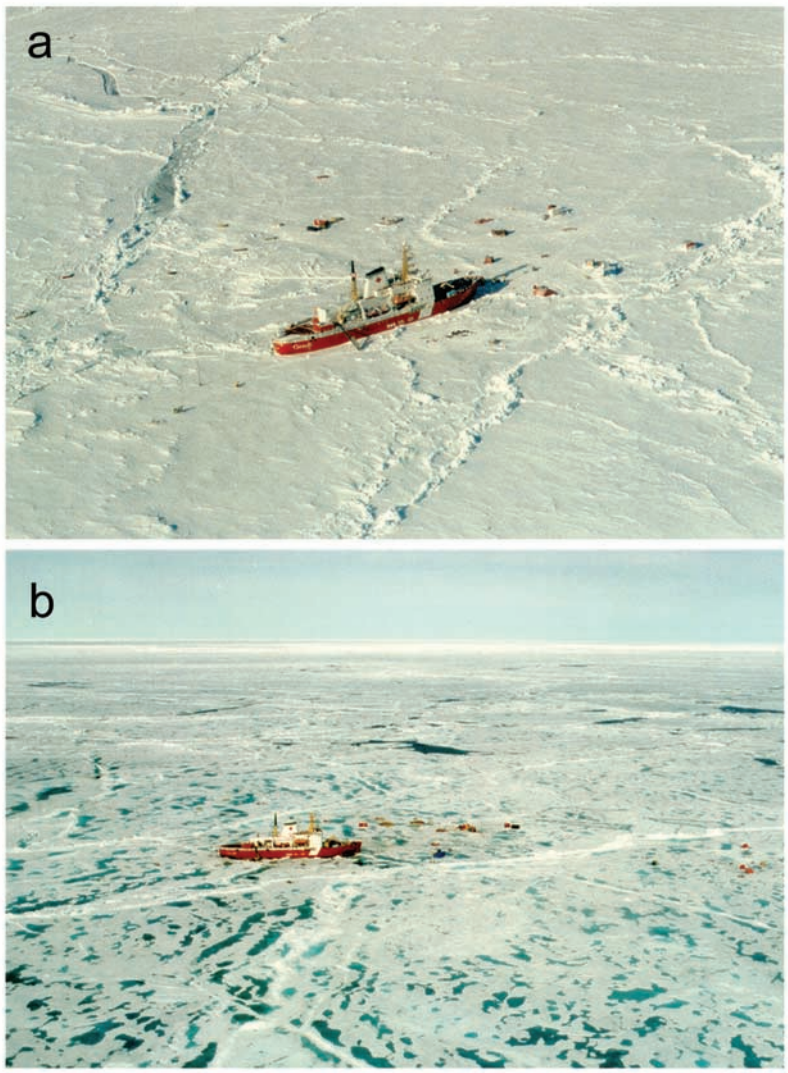

Figure 1. Aerial view of Ice Station SHEBA in April 1998 (top) and July 1998 (bottom). Surface conditions changed from uniform snow-covered ice to a mixture of ponds, ice, and open water. The ship is the Canadian Coast Guard icebreaker *Des Groseilliers*.

ice. They have established a qualitative understanding of how changes in the physical properties of the ice and snow cause changes in the optical properties and the albedo. What is lacking in these studies, however, is a systematic time series relating the seasonal evolution of albedo to changes in the surface conditions and physical properties of the interior of the ice. Because the optical properties of ice and snow as well as the incident solar irradiance are strong functions of wavelength, detailed wavelength-dependent observations are needed to determine the energy deposition properly. In this paper we present such a systematic time series and demonstrate how the seasonal evolution of albedo is directly linked to physical changes in the ice cover during melt and freeze-up.

2. Experimental Approach

[6] As part of the ice albedo feedback studies carried out during the 1997–1998 Surface Heat Budget of the Arctic Ocean (SHEBA) field experiment [*Perovich et al.*, 1999], we measured spectral and wavelength-integrated albedos together with other components of the heat and mass balance. Albedos were monitored at a wide variety of sites selected to include all available multiyear ice types and conditions, from ponded ice to thick, snow-covered ice. To investigate spatial and temporal changes on a single floe, regular surveys of albedo were made every few meters along a 200-m-long "albedo line" (see Figure 2). These surveys were repeated weekly in April and May, when changes in surface conditions and ice properties were slow, and every other day during June, July, and August, when changes were rapid and the impact of ice albedo feedback was large. Data from these observations are available on a CD-ROM [*Perovich et al.*, 1999].

[7] The albedo at a particular wavelength (λ) is

$$\alpha(\lambda) = \frac{F_{\uparrow}(\lambda)}{F_{\downarrow}(\lambda)}. \quad (1)$$

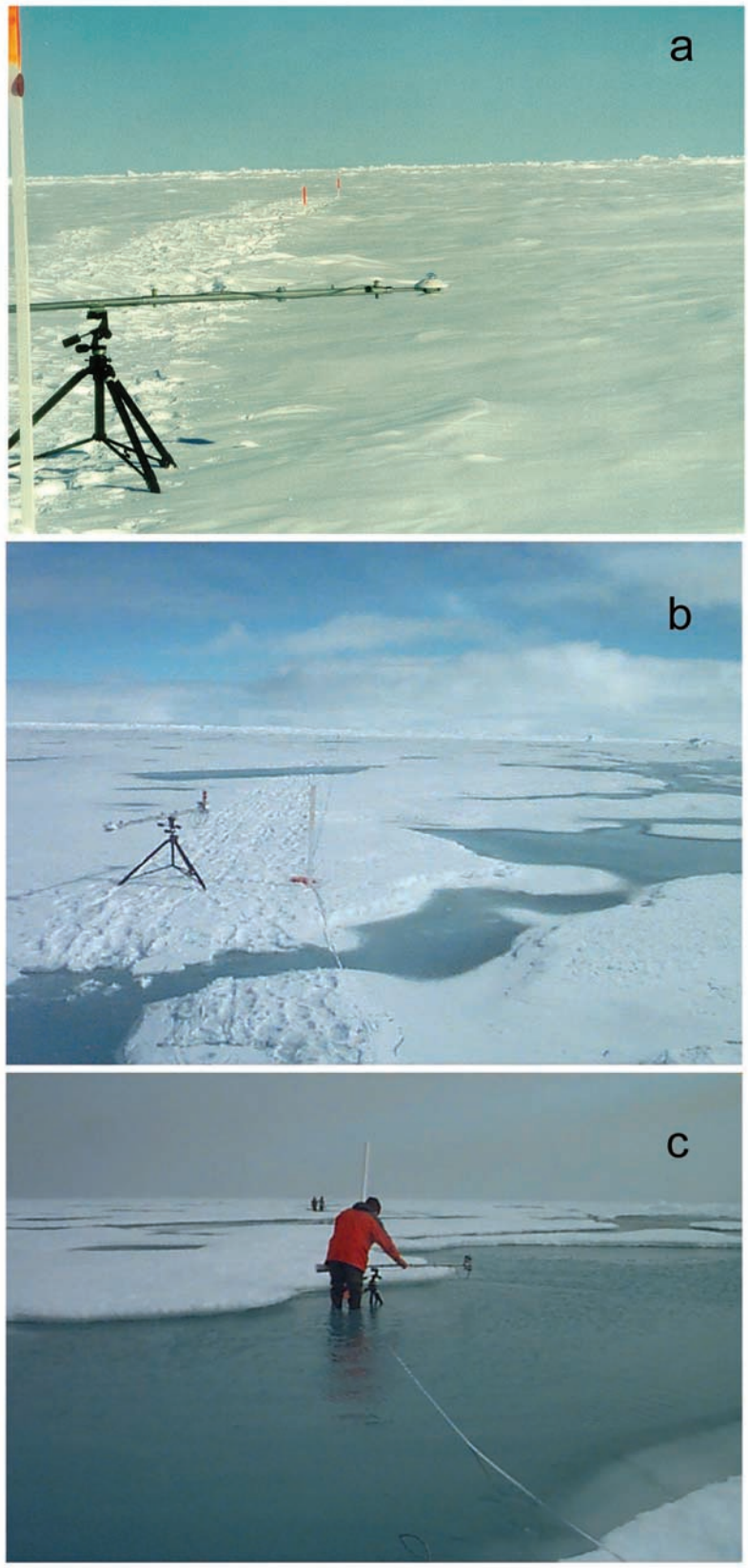

Figure 2. Surface conditions along the albedo line on (top) 17 April 1998, (middle) 25 June 1998, and (bottom) 4 August 1998.

Table 1. Characteristics of Optical Instruments Used in This Experiment

Instrument	Type	Wavelength Range, nm	Spectral Resolution	Cosine Collector
Kipp & Zonen albedometer	radiometer	300–3000 nm	wavelength-integrated	flat plate
Eppley Lab. Inc. Model PSP	radiometer	300–3000	wavelength-integrated	flat plate
Spectron Engineering SE-590 UV	spectroradiometer	300–400	3 nm	integrating sphere
Spectron Engineering SE-590 VIR	spectroradiometer	400–1000 nm	3 nm	diffusing dome
Spectron Engineering SE-590 IR	spectroradiometer	1000–2300 nm	20 nm	integrating sphere

The wavelength-integrated, or total, albedo (α_t) is the ratio of the reflected irradiance ($F_\uparrow$) to the incident irradiance ($F_\downarrow$), which can be expressed as

$$\alpha_t = \frac{\int_{300}^{3000} \alpha(\lambda) F_\downarrow(\lambda) d\lambda}{\int_{300}^{3000} F_\downarrow(\lambda) d\lambda}, \quad (2)$$

where the limits of integration span the incident solar spectrum.

[8] Albedos along the 200-m line were measured using five different field-portable spectroradiometers and shortwave radiometers. The spectrophotometers were diode array instruments with rapid response times, so that a full spectral region could be measured in a few seconds. At a given site, it typically took less than a minute to measure the pair of incident and reflected irradiance spectra needed to compute the albedo. Hemispherical and integrating sphere cosine collectors were used to obtain the appropriate instrument field of view for irradiance measurements. Spectral resolution was 3 nm in the UV, visible and near infrared, and 20 nm at wavelengths above 1000 nm. Calibration and intercomparison of these instruments were performed in the field. The detectors were mounted on a 1.5-m-long arm to minimize shadowing of the surface (Figure 2). The arms were mounted on a tripod for easy and accurate leveling. The specifications of the five instruments used to make the albedo measurements are summarized in Table 1.

[9] The albedo measurements were supplemented with a description of the physical properties of the ice cover. The focus was on characterizing the surface conditions, since they have the greatest influence on albedo [*Grenfell and Maykut*, 1977; *Perovich*, 1996; *Allison et al.*, 1993]. We monitored the snow coverage and depth, the pond fraction and depth, and the evolution of the surface scattering layer. Photographs were taken to document changes in surface conditions. Because of concerns that soot released from the ship might affect the albedo and seasonal melt cycle, a detailed survey was carried out to determine the level of contamination in the spring followed by spot checks during the summer [*Grenfell et al.*, 2002]. These measurements indicated that soot contamination from the ship was approximately 5 ngC/g in the areas where the measurements were made. This value is a factor of 3 below the threshold value for which the albedo at 500 nm is reduced by 0.01 [*Grenfell et al.*, 1994], so that there was no significant effect on the springtime albedo or its subsequent seasonal evolution.

3. Results

[10] Significant changes occur in the ice cover during the summer melt season, as the photographs in Figure 2 illustrate. During April the ice was covered by an optically thick layer of cold, dry snow (Figure 2a), creating a bright, white, and uniform-appearing surface. At this time, snow depths along the albedo line ranged from 8 to 54 cm, averaging 28 cm. By 25 June, most of the snow cover

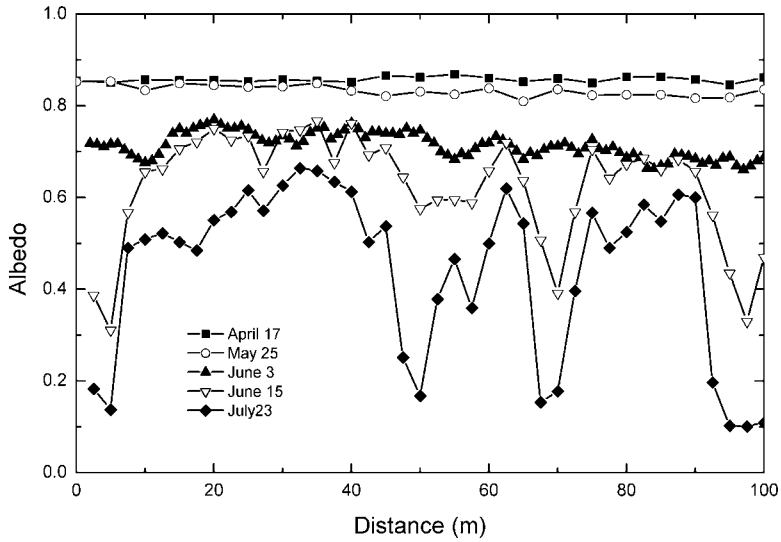

Figure 3. Spatial and temporal variability of wavelength-integrated albedo along the albedo line during the melt season.

Figure 4. Melt pond appearance in its early stage, 29 June (top) and fully mature, 8 August (bottom).

had melted, and the surface was a mix of bare ice with a few shallow melt ponds (Figure 2b). Another month of melting dramatically changed surface conditions. By 4 August (Figure 2c), the snow was completely gone, and the surface was either bare ice or melt ponds. The ponds were ubiquitous and at their maximum extent covered more than 20% of the surface area of the ice floes.

[11] These photographs illustrate the magnitude of the changes associated with the summer melt season and provide a qualitative sense that the surface grew darker and more spatially variable as melt progressed. This observation is confirmed quantitatively by the albedo measurements. The evolution of wavelength-integrated albedos along the first 100 m of the albedo line is displayed in Figure 3. The cold snow-covered ice of 17 April has a high albedo (0.82–0.88) and is spatially uniform. This persisted for the next several weeks. By 25 May, no melting had occurred and the snow was still dry. Snow metamorphism during this time resulted in slightly larger grain sizes and a slight decrease in albedo. Albedos were still spatially uniform. Rain on 29 May marked the beginning of the melt season and a transition from dry snow to wet, melting snow. Albedos from 3 June show a drop to wet snow values of 0.7–0.75. In some places the snow was no longer optically thick, resulting in a modest amount of spatial variability in albedo ($\sim$0.1). Melting of the snowpack continued and by 15 June the albedo line consisted of melting snow, bare melting ice, and a few melt ponds. Spatial variability along the line increased greatly, with albedos ranging from 0.3 for the ponds to 0.7 for the melting snow. As the melt season progressed, the snow cover disappeared, the bare ice developed a melting surface granular layer, and the ponds grew deeper and wider. By 23 July, albedos had decreased everywhere, and the spatial variability had increased, from a minimum of 0.1 for the deep, dark melt ponds to a maximum of 0.65 for bare, white ice.

3.1. Albedos of Ice and Ponds

[12] As the snow melted, the ice followed one of two evolutionary sequences, eventually becoming either bare ice

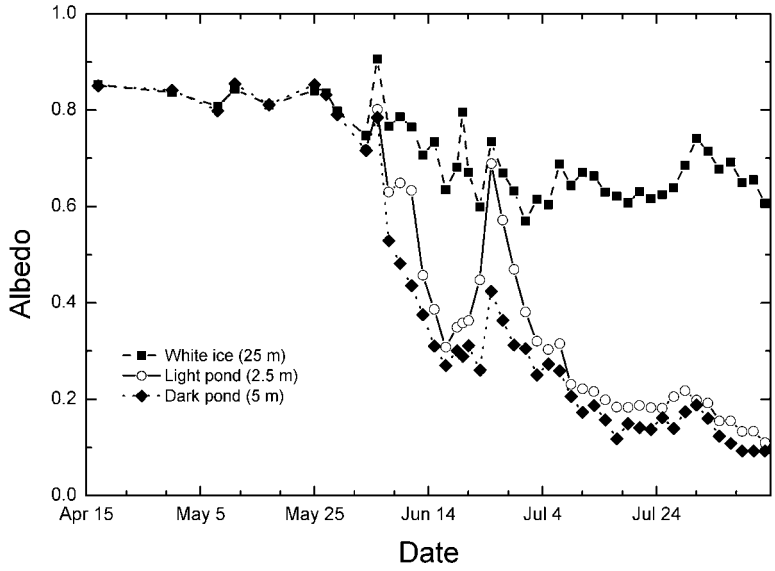

Figure 5. Time series of wavelength-integrated albedo at selected sites along the albedo line.

or pond-covered ice. The development of melt ponds is evident at several locations along the albedo line (5, 50, 70, and 100 m). Ponds persisted in the location where they first formed and grew deeper and wider throughout the summer. Figure 4 shows the development of a melt pond from 29 June to 8 August. A large change in size is evident for the melt pond in Figure 4. This particular pond had a portion with a light bottom and a portion with a dark bottom. The water depth was the same in both sections, but the properties of the underlying ice differed: the ice in the lighter section had many more air bubbles than the darker section. Note that while the pond changes significantly, there is little change in the appearance of the bare, white ice between the photographs in Figure 4.

3.1.1. Wavelength-Integrated Albedo

[13] Figure 5 shows time series of wavelength-integrated albedos from white ice and the light and dark areas of the pond in Figure 4. Albedos at the sites began to differ significantly after just a few days of melting in early June. The white ice site remained snow covered with a melting snow albedo of 0.7 to 0.8. At this stage, the light pond was bare melting ice with an albedo of 0.65, and the dark pond was already covered by a few centimeters of water, with an albedo of 0.5. Albedos continued to decrease at the pond sites as the ponds got deeper. At the bare ice site, all the snow melted, reducing the albedo to 0.6–0.7. On 26 June there was an increase in albedo at all three sites due to a brief cold spell when an ice skim formed on some of the

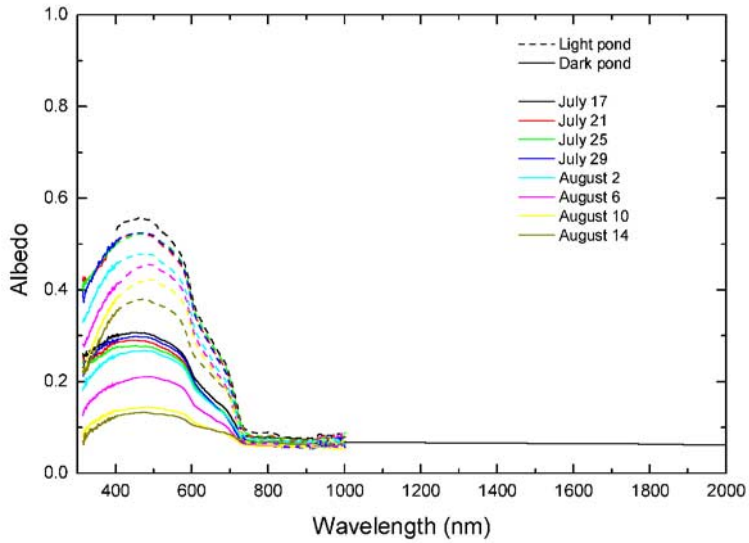

Figure 6. The evolution of the spectral albedo for the light portion and dark portion of a melt pond from 17 July until just before freeze-up.

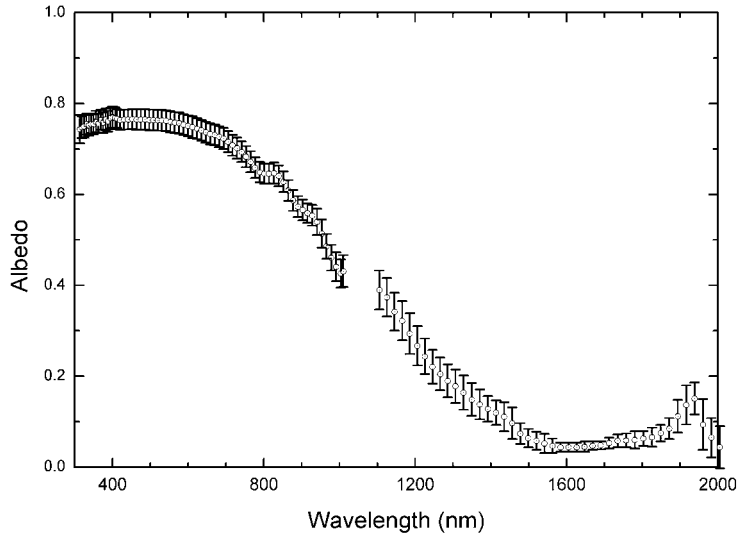

Figure 7. Spectral albedos of bare, white ice during the melt season from 7 July through 12 August. The circles denote the mean of all the albedos measured at each wavelength during this period, and the bars show the range.

ponds and there was 1 cm of new snow. The increase was greatest at the light pond site where the albedo jumped from 0.3 to 0.7 as the surface conditions changed from a melt pond to ice with a thin snow cover. After this, the pond albedos decreased throughout the rest of the summer, reaching a minimum value of 0.1 on 13 August. By this time most of the bubbly ice in the light pond had melted, and there was little difference between the light and dark portion of the pond.

3.1.2. Spectral Albedos

[14] Throughout the summer (early July through mid-August), the albedo of bare ice was fairly constant (0.6–0.7), but there was a progressive decrease in the albedo of ponded ice. Spectral albedos from 17 July through 14 August for the light and dark portions of the pond are plotted in Figure 6. There was little variability in albedo in the near infrared at wavelengths beyond 750 nm, where the absorption in the water is so great that the underlying ice does not contribute to the albedo. The small differences in albedo ($\sim$0.05) are due to minor variations in the sky conditions and the water roughness at the pond's surface. Differences were considerable at visible wavelengths (400–750 nm). In particular, from 400 to 600 nm light pond albedos were 0.2 to 0.25 larger than dark pond values. The scattering of the underlying ice has the greatest influence on albedo from 400 to 600 nm, where the pond water is the most transparent [*Grenfell and Perovich*, 1984]. For both the light and dark portion of the pond, there was a steady decrease in albedo of 0.15 to 0.2 between 17 July and 14 August. This occurred as melting deepened the ponds and thinned the scattering layer of the underlying ice.

[15] Spectral albedos measured at the bare ice site on 12 days between 7 July and 12 August are plotted in Figure 7. The circles denote the mean of all the albedos measured at each wavelength during this period and the bars denote ±1 standard deviation. The albedo curve is high (0.7 to 0.8) and flat across the visible, giving a white appearance to the ice, and decreasing in the near infrared. The spectral shape is the same for all of these curves. As the small size of the bars indicates, there was tight clustering of the white ice albedos. During this five-week period, the albedo at a particular wavelength never varied by more than 0.1. The same was true for the total albedo of the bare ice. There was approximately 60–70 cm of surface ablation, yet no systematic change in albedo. For white ice, the albedo is dominated by scattering in a few-centimeter-thick surface scattering layer of granular, decomposing ice. As the melt season progressed, this layer kept renewing itself due to melting within the near-surface portion of the ice, resulting from ongoing radiation absorption in the upper layers of the ice [*Perovich et al.*, 2001]. The changes that did occur in the albedo of the bare ice were fluctuations, which we believe where due to variations in the thickness of this surface layer. Foggy days, with condensation melting on the surface, tended to thin the scattering layer, and sunny days, with larger fluxes of penetrating solar irradiance, tended to increase the layer thickness.

[16] The large disparity between melt pond and bare ice albedos is due to differences in the light-scattering properties of the surface layer. For bare ice, the water has drained from the surface, leaving a few-cm-thick, granular surface scattering layer, with 10–20 cm of bubbly ice below. Variations in the scattering properties of the bubbly ice are determined by the number and size distribution of vapor bubbles.

3.2. Areally Averaged Albedos

[17] From a large-scale modeling, or climate, perspective, the interest is not so much in the evolution of a single melt pond, or a piece of ice, but the ensemble of ponds and ice that comprise the ice cover. The key issue is how the albedo of that ensemble is evolving. From the previous discussion, we know that during the course of the melt season pond albedos decreased and white ice albedos remained relatively

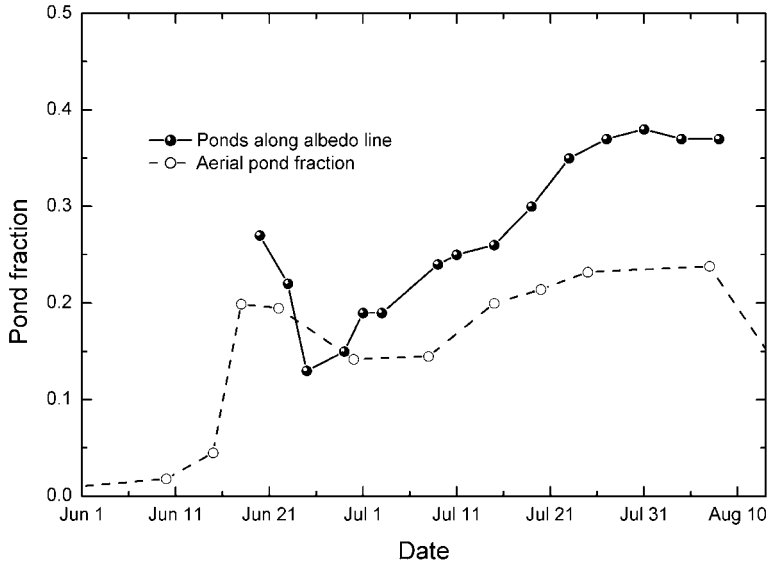

Figure 8. Time series of the fractional area of the ice covered by melt ponds as measured along the albedo line and from aerial photographs.

constant. Figure 8 shows the fraction of the albedo line that was pond-covered throughout the summer. Also plotted is a larger-scale estimate of the fraction of the ice covered by ponds, which was determined by analyzing aerial photographs [*Eicken et al.*, 2002; *Perovich et al.*, 2002]. Though the albedo line had a larger pond fraction than the general SHEBA region, both the surface-based and aerial observations exhibited the same temporal dependence. The temporal increase in pond fraction indicates a seasonal reduction of the areally averaged albedo [*Perovich et al.*, 1999; *Perovich et al.*, 2002]. In addition, the lead fraction was 3–5% from May through July then jumped to 20% in early August [*Perovich et al.*, 2002]. Since the average lead albedo was quite small, 0.066 [*Pegau and Paulson*, 1999], an increase in open water would reduce the overall albedo of a region.

3.2.1. Wavelength-Integrated Albedo

[18] We examined the evolution of the albedo of the ice cover by averaging the individual measurements along the albedo line to derive an areally averaged albedo and a standard deviation for each day. Although the albedo line did not include any open water, we believe that the evolution of the albedo line was generally representative of the multiyear portion of the ice cover. During melt, other

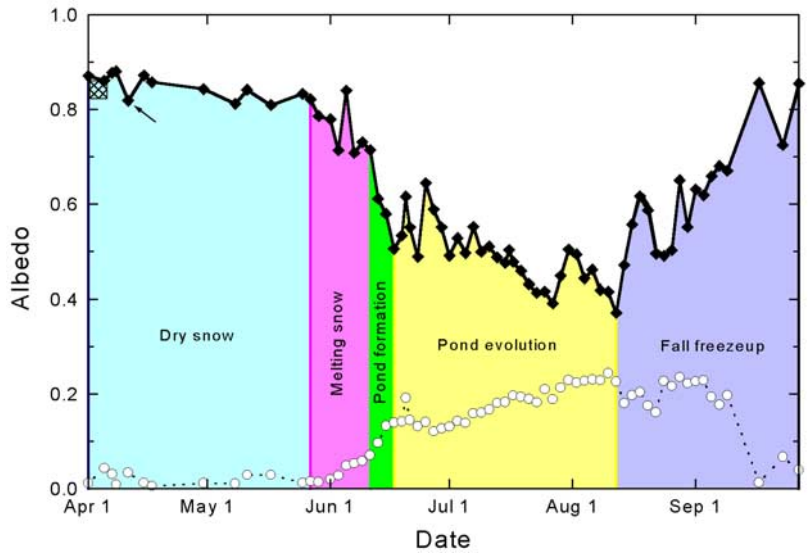

Figure 9. Time series of wavelength-integrated albedo from 1 April 1998 through 27 September 1998. Values are averaged over a 200-m-long albedo line. The arrow points to 17 April when the sky was clear. Also plotted is the albedo measured at the beginning of the experiment in October 1997 (solid squares). The standard deviation of albedo measured along the albedo line for each is plotted as open circles.

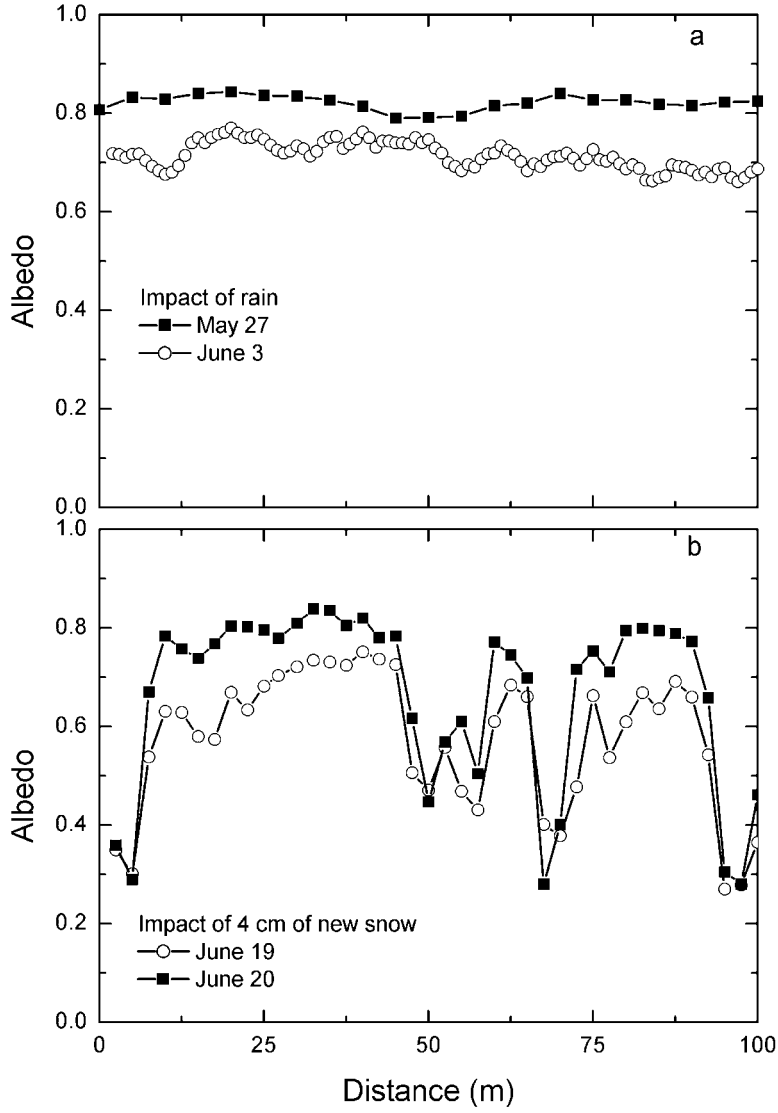

Figure 10. Influence of synoptic events on albedo. Observations along the albedo line (a) before and after the first rainfall of summer and (b) before and after a 4-cm snowfall in June.

regions of the ice cover may have a different mix of ponds and bare ice, but that would only change the magnitude of the average albedo, not the character of the temporal evolution of albedo.

[19] The areally averaged albedo time series (Figure 9) is divided into five sections denoting the distinct phases of the seasonal evolution of albedo: dry snow, melting snow, pond formation, pond evolution, and fall freeze-up. These five phases were defined by our observations of the physical state of the snow and ice. In the first phase (April–May), the albedo was high (0.8–0.9) and spatially uniform. These values were comparable to albedo measurements made of snow-covered ice during the previous October (0.82–0.85). During this time there was a slight and gradual decrease in albedo as the snow cover warmed and the snow grain size increased. The rain of 29 May initiated phase 2, causing rapid coarsening of the snow to about 1 mm diameter, resulting in a drop in the average albedo from 0.8 to 0.7. As the snow cover melted, there was more spatial variability in the albedo, as evidenced by the increase in the standard deviation. Phase 3 started in mid-June, when melt pond formation resulted in a sharp drop in albedo from 0.7 to 0.5 in only a week. After this sharp drop associated with the appearance of melt ponds, there was a long period of a slow, steady decline in albedo as the melt ponds grew deeper and larger in areal extent. Even though the melt season was under way, there were still occasional periods of cooler temperatures and light snow during the next two weeks, with attendant increases in albedo. By early August, the average albedo along the line was only 0.4. The spatial variability of albedo was greatest at this time, ranging from 0.1 to 0.65 with a standard deviation of 0.25 along the line. Starting in late July and early August, there were brief, intermittent periods with air temperatures below freezing. During these periods, ice skims formed on the surface of ponds and there were occasional snow flurries, resulting in an increase of 0.1 in average albedo. Again there were a few weeks of ''flickering'' during freeze-up, with albedos

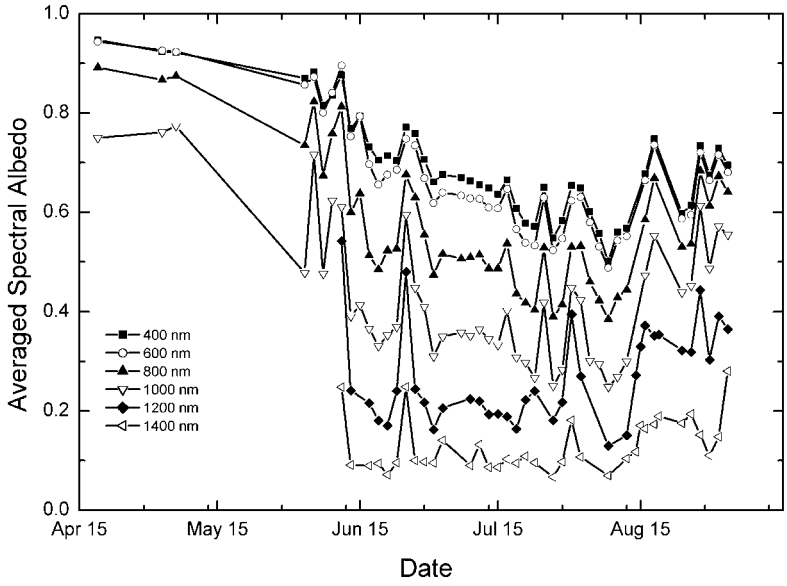

Figure 11. Time series of spectral albedo averaged over 100-m-long line at selected wavelengths as indicated in the legend.

increasing and decreasing depending on the synoptic weather. By the end of August, surface temperatures were consistently below freezing and the albedo increased as the snow cover got deeper. By the end of September, average albedos returned to their springtime maxima of 0.8 to 0.9 and were spatially uniform.

[20] The effects of synoptic weather events, such as rain and snow, on albedo are illustrated in Figure 10. The first rainfall of the year on 29 May changed surface conditions from dry snow to wet snow, resulting in a 0.05 to 0.15 decrease in albedo. Larger decreases in albedo occurred in areas of thinner snow, where the wet snow was no longer optically thick. On 19 June we received 4 cm of new wet snow, which caused an increase in albedo for bare ice of about 0.2 to a value of 0.8. On ponded ice, new snow either melted or formed a slushy surface layer with little effect on the albedo. The increase in albedo was ephemeral, as the snow quickly melted, and on 21 June albedos were back to 19 June values.

[21] Another potential source of variability in the wavelength-integrated albedo is changes in the incident solar spectrum due to cloudiness [*Grenfell and Maykut*, 1977; *Grenfell and Perovich*, 1984]. Calculations [*Grenfell and Perovich*, 1984] indicate that for a given surface the albedo is 5–10% greater on a cloudy day than on a clear day. The cloud impact was minor in our observations, since for the most part our albedos were measured under cloudy skies. One exception occurred on 17 April (arrow in Figure 9), when the measurements were made under clear skies. This decrease was due to measuring under clear sky conditions, not to a change in surface conditions.

3.2.2. Spectral Albedo

[22] The temporal evolution of areally averaged spectral albedos is similar to the wavelength-integrated counterparts. Areally averaged spectral albedos were computed by averaging measurements along the first 100 m of the albedo line (Figure 11). Decreases in albedo were more rapid and larger in magnitude at near-infrared wavelengths than at visible wavelengths, reflecting the influence of the melt ponds versus bare and snow-covered ice. For ponded areas, the spectral gradient between 500 and 1000 nm is much stronger than for the other ice types, so the separation increases and the magnitudes decrease as the ponds develop (mid-June) and evolve (July).

3.3. Aircraft Albedo

[23] To extend local scale observations to larger scales, broadband radiation measurements were obtained aboard the University of Washington's (UW) Convair-580 research aircraft using two identical Eppley radiometers, one pointing up and one down. These instruments provided measurements of upwelling and downwelling radiation at visible and near-IR wavelengths (300–3000 nm) from which the surface albedo was calculated.

[24] Aircraft albedo measurements were obtained over the albedo line on seven occasions between 30 May and 23 June 1998. Straight and level runs of the aircraft were made over the length of the albedo line to determine the average albedo. The flights were made at ~90–600 m above the surface and below cloud base (if cloud was present, which it generally was). The data were screened to include only those values for which: (1) there was little or no cloud between the aircraft and the underlying surface; and (2) the pitch and roll angles of the aircraft were less than 5° in either direction.

[25] The airborne measurements showed that the average surface albedo of the CRREL albedo line decreased from ~0.8 to ~0.6 during the period 30 May to 23 June. This was a period of significant transition as the surface changed from snow covered to heavily ponded. For a radiometer with a cosine collector as its foreoptics, 90% of the signal is from a circle with a radius approximately twice the height of the instrument. For the surface-based measurements this field of view has a radius of 2 m, while for the aircraft

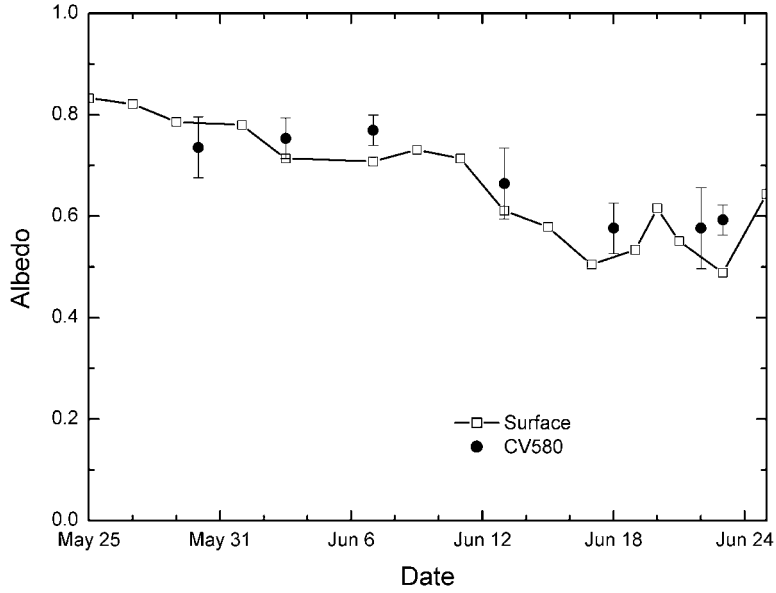

Figure 12. Comparison of the broadband (300–3000 nm) albedo averaged on the albedo line measured from the University of Washington Convair-580 aircraft and from the surface. Error bars of one standard deviation are plotted for the aircraft results.

measurements the radius was much larger; between 200 and 1200 m. Even though the "footprints" were quite different, the albedo values from the airborne measurements are in good agreement with the ground-based measurements of daily average albedo over the albedo line during this period of significant spatial and temporal variability (Figure 12). The temporal trends were the same for surface and aircraft albedos. Aircraft values were slightly larger since their footprint included the unponded flank of a major pressure ridge. This agreement supports two points: (1) surface measurements along the albedo line are indeed representative of an area, not just a line, and (2) aircraft-based radiometers provide a means of measuring albedo on larger scales.

4. Discussion

[26] Time series observations of total albedo are available from an analysis of the Soviet NP drifting station measurements from 1950 through 1991 [*Radionov et al.*, 1997]. These data represent a very large statistical sample, though they have a rather coarse temporal resolution and only a

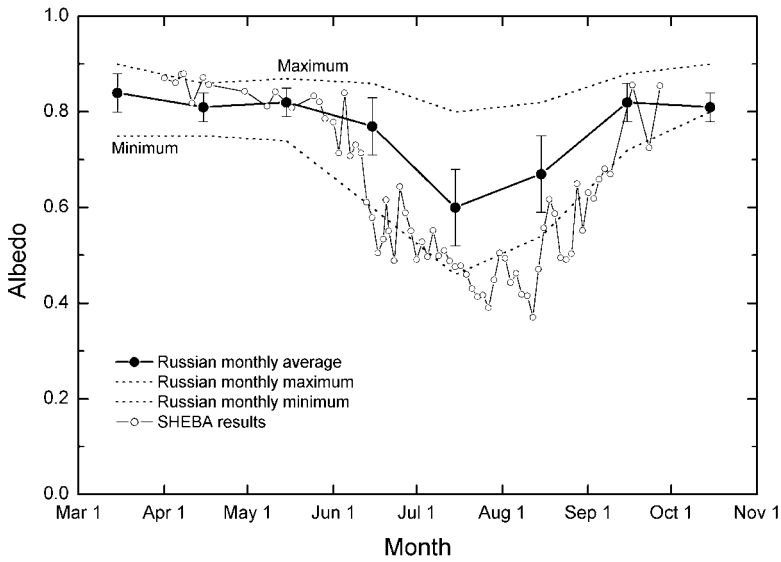

Figure 13. Annual variations in wavelength-integrated albedo from Soviet NP drift stations and SHEBA.

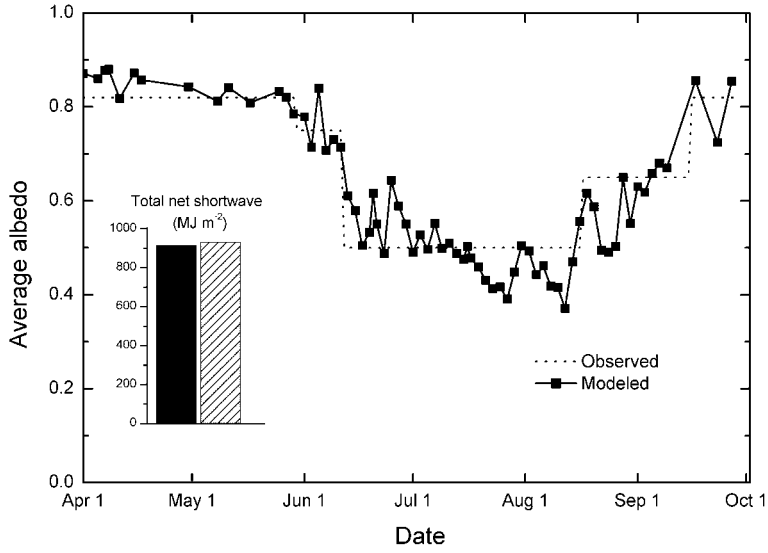

Figure 14. Comparison of observed and simulated model values of wavelength-integrated albedo.

very brief characterization of the physical properties evolution. They report maximum values of 90% and minimum values near 45%. Their time series consist of multiyear averages of observations grouped by month (Figure 13). Since these series do not include open water and thus represent 100% ice cover, they can be compared directly with the albedo averages for our albedo line (Figure 9).

[27] Due to the vigorous SHEBA melt season, the summer drop-off is sharper for the SHEBA data, and the albedos are at the lower end of, or below, the Russian results. The Russian data show the minimum albedo in July (0.6 ± 0.08), while we find a minimum in mid-August with values around 0.4 to 0.5. In the Russian data, the results of flickering are contained in the error limits and smoothed out by averaging over many years. They report that there is no significant multiyear trend in the annual pattern. The increased prominence both in amplitude and duration for the summer reduction of total albedo in the SHEBA data set is a strong indicator of the increase in intensity and duration of the summer melt season of 1998.

[28] The timing and amplitude of the summer albedo phases will depend on location and year, but we believe that the form of annual cycle of albedo will be the same. The time series of areally averaged albedo in Figure 9 defines the key factors governing the annual cycle of albedo. Determining the timing of each of the five phases is critical to accurately represent the albedo. To determine the amplitude of the albedo cycle, we need to know the time series of pond fraction and lead fraction, as well as a measure of the pond evolution.

[29] There are several different albedo parameterizations in use in large-scale sea ice models and in general circulation models (GCMs). These parameterizations range in complexity, relating albedo to surface temperature [*Hibler*, 1980; *Ingram et al.*, 1989; *Ross and Walsh*, 1987], ice thickness [*Bitz et al.*, 1996; *Flato and Brown*, 1996; *Battisti et al.*, 1997], and ice type [*Schramm et al.*, 1997]. *Curry et al.* [2001] used a single-column model along with results from SHEBA and FIRE [*Curry et al.*, 2000] to evaluate albedo parameterizations. They conclude that, for climate applications, the albedo should be related to the characteristics of the surface (snow depth, ice thickness, pond fraction, ice concentration).

[30] For purposes of illustration, consider the Climate System Model GCM [*Weatherly et al.*, 1998]. This model uses four levels to represent the ice albedo: 0.82 for cold snow, 0.75 for melting snow, 0.5 for melting ice, and 0.65 for cold ice. Figure 14 compares the time series of observed albedo with the four-level parameterization. When there is a cold or a melting snow cover present, observed and modeled albedo agree nicely. However, once the ponds begin to form, the values differed for the remainder of the summer, with the modeled albedo first less than the observed, then greater. There was a similar deviation during freeze-up, though in this case the model albedo was first greater than observed, then less. Differences were typically less than 0.1.

[31] From a large-scale modeling perspective, it is neither practical nor critical to model the time series of albedo exactly. It is important to estimate accurately the total solar heat input into the ice cover. We multiplied both the observed and modeled albedos from Figure 14 with the incident solar irradiance measured at SHEBA (R. Moritz, personal communication, 1999) to determine the net input of solar irradiance from April through September. The net solar irradiance was 914 MJ m^{-2} using the observed albedos and 930 MJ m^{-2} using the model albedos, a difference of less than 2%. This agreement between observed and modeled values is not just fortuitous, it is due primarily to the proper selection of the transition points for changes in albedo. To represent the albedo accurately, a model must correctly determine the onset of melt, the time of melt pond formation, the duration of melt, and the start of fall freeze-up.

5. Conclusions

[32] During the SHEBA field experiment, the spatial variability and temporal evolution of the albedo of Arctic

sea ice was monitored over an entire annual cycle. For more than nine months of the year, the albedo of the ice cover is high (0.8–0.9) and spatially uniform, but in summer the albedo of the ice cover decreases and the spatial variability of albedo increases. Over distances of only a few meters, albedos can vary from 0.1 for leads to 0.2 for dark ponds to 0.4 for light ponds to 0.6–0.7 for melting multiyear ice.

[33] Examining individual ice types, the albedo of bare, multiyear ice changed little during the melt season, because the highly scattering surface layer continually renewed itself. The behavior of melt ponds was quite different. Throughout the summer, melt pond albedos continually decreased as the ponds grew wider and deeper and the underlying ice thinned.

[34] The evolution of the areally averaged albedo was a combination of a smooth seasonal trend with synoptic fluctuations. There were five distinct phases of the seasonal evolution: dry snow (~0.8–0.9), melting snow (decrease from 0.8 to 0.7), pond formation (decrease from 0.7 to 0.5), pond evolution (decrease from 0.5 to 0.4), and fall freeze-up (increase from 0.4 to 0.8). Superposed on this smooth season trend were abrupt fluctuations due to synoptic weather events, such as rain or snow. While the synoptic events typically were short-lived, they did cause brief changes in albedo of 0.1–0.2. Their impact was greatest near the onsets of summer melt and fall freeze-up.

[35] Progressive reduction in the average albedo of individual floes during the summer was due primarily to changes in the coverage and optical properties of the melt ponds. However, changes in the regional albedo can also be influenced by the increase in the amount of open water resulting from divergence of the ice pack and from lateral melting on floe edges.

[36] **Acknowledgments.** The authors thank J.A. Richter-Menge, W.B. Tucker III, B. Elder, H. Bosworth, and J. Ukita for their capable assistance in the field measurements. We also thank the crew of the *Des Groseilliers* and the SHEBA Logistics Office for their excellent support. Thanks are due to Joanne Kang for help in reducing the airborne data. SHEBA was sponsored by the National Science Foundation Office of Polar Programs and the Office of Naval Research High Latitude Physics Program. This work was funded under Office of Naval Research grant N00014-97-1-0765 and NSF grant OPP-980816. One of the authors (D. Perovich) was also supported by Department of the Army and NASA projects.

References

Allison, I., R. E. Brandt, and S. G. Warren, East Antarctic sea ice: Albedo, thickness distribution, and snow cover, *J. Geophys. Res.*, *98*, 12,417–12,429, 1993.

Battisti, D. S., C. M. Bitz, and R. E. Moritz, Do general circulation models underestimate the natural variability in the Arctic climate?, *J. Clim.*, *10*, 1909–1920, 1997.

Bitz, C. M., D. S. Battisti, R. E. Moritz, and J. A. Beesley, Low-frequency variability in the Arctic atmosphere, sea ice, and upper-ocean climate system, *J. Clim.*, *9*, 394–408, 1996.

Buckley, R. G., and H. J. Trodahl, Thermally driven changes in the optical properties of sea ice, *Cold Reg. Sci. Technol.*, *14*, 201–204, 1987.

Curry, J. A., J. L. Schramm, and E. E. Ebert, On the sea ice albedo climate feedback mechanism, *J. Clim.*, *8*, 240–247, 1995.

Curry, J. A., et al., FIRE Arctic clouds experiment, *Bull. Am. Meteorol. Soc.*, *81*, 5–30, 2000.

Curry, J. A., J. L. Schramm, D. K. Perovich, and J. O. Pinto, Applications of SHEBA/FIRE data to evaluation of snow/ice albedo parameterizations, *J. Geophys. Res.*, *106*, 15,345–15,355, 2001.

Dickinson, R. E., G. A. Meehl, and W. M. Washington, Ice-albedo feedback in a CO_2-doubling simulation, *Clim. Change*, *10*, 241–248, 1987.

Eicken, H., H. R. Krouse, D. Kadko, and D. K. Perovich, Tracer studies of pathways and rates of meltwater transport through Arctic summer sea ice, *J. Geophys. Res.*, *107*, doi:10.1029/2000JC000583, in press, 2002.

Flato, G. M., and R. D. Brown, Variability and climate sensitivity of landfast Arctic sea ice, *J. Geophys. Res.*, *101*, 25,767–25,777, 1996.

Grenfell, T. C., and G. A. Maykut, The optical properties of ice and snow in the Arctic Basin, *J. Glaciol.*, *18*, 445–463, 1977.

Grenfell, T. C., and D. K. Perovich, Spectral albedos of sea ice and incident solar irradiance in the Southern Beaufort Sea, *J. Geophys. Res.*, *89*, 3573–3580, 1984.

Grenfell, T. C., S. G. Warren, and P. C. Mullen, Reflection of solar radiation by the Antarctic snow surface at ultraviolet, visible, and near-infrared wavelengths, *J. Geophys. Res.*, *99*, 18,669–18,684, 1994.

Grenfell, T. C., B. Light, and M. Sturm, Spatial distribution and radiative effects of soot in snow and sea ice during the SHEBA experiment, *107*(10), 10.1029/2000JC000414, in press, 2002.

Hibler, W. D., Modeling a variable thickness sea ice cover, *Mon. Weather Rev.*, *108*, 1943–1973, 1980.

Ingram, W. J., C. A. Wilson, and J. F. B. Mitchell, Modeling climate change: An assessment of sea ice and surface albedo feedbacks, *J. Geophys. Res.*, *94*, 8609–8622, 1989.

Langleben, M. P., Albedo and degree of puddling of a melting cover of sea ice, *J. Glaciol.*, *8*, 407–412, 1969.

Langleben, M. P., Albedo of melting sea ice in the southern Beaufort Sea, *J. Glaciol.*, *10*, 101–104, 1971.

Maykut, G. A., and N. Untersteiner, Some results from a time dependent, thermodynamic model of sea ice, *J. Geophys. Res.*, *76*, 1550–1575, 1971.

Pegau, W. S., and C. A. Paulson, The effect of clouds on the albedo of Arctic leads, *Eos Trans. AGU*, *80*(46), Fall Meet. Suppl., Abstract F221, 1999.

Perovich, D. K., Seasonal changes in sea ice optical properties during fall freeze-up, *Cold Reg. Sci. Technol.*, *19*, 261–273, 1991.

Perovich, D. K., Light reflection from sea ice during the onset of melt, *J. Geophys. Res.*, *99*, 3351–3359, 1994.

Perovich, D. K., The optical properties of sea ice, *U. S. Cold Reg. Res. and Eng. Lab. Monogr. 96-1*, 25 pp., Hanover, N. H., May 1996.

Perovich, D. K., C. S. Roesler, and W. S. Pegau, Variability in sea ice optical properties, *J. Geophys. Res.*, *103*, 1193–1209, 1998.

Perovich, D. K., T. C. Grenfell, B. Light, J. A. Richter-Menge, M. Sturm, W. B. Tucker III, H. Eicken, G. A. Maykut, and B. Elder, SHEBA: *Snow and Ice Studies* [CD-ROM], U.S. Army Cold Reg. Res. and Eng. Lab., 1999.

Perovich, D. K., J. A. Richter–Menge, and W. B. Tucker III, Seasonal changes in sea ice morphology, *Ann. Glaciol.*, *33*, 171–176, 2001.

Perovich, D. K., W. B. Tucker III, and K. A. Ligett, Aerial observations of the evolution of ice surface conditions during summer, *J. Geophys. Res.*, *107*, doi:10.1029/2000JC000449, in press, 2002.

Radionov, V. F., N. N. Bryazgin, and E. I. Alexandrov, The snow cover of the Arctic Basin, *APL-UW Tech. Rep. 9701*, Univ. of Wash., Seattle, Feb. 1997.

Ross, B., and J. E. Walsh, A comparison of simulated and observed fluctuations in summertime Arctic surface albedo, *J. Geophys. Res.*, *92*, 13,115–13,125, 1987.

Schramm, J. L., M. M. Holland, and J. A. Curry, Modeling the thermodynamics of a sea ice thickness distribution, 1, Sensitivity to ice thickness resolution, *J. Geophys. Res.*, *102*, 23,079–23,091, 1997.

Spelman, M. J., and S. Manabe, Influence of oceanic heat transport upon the sensitivity of a model climate, *J. Geophys. Res.*, *89*, 571–586, 1984.

Washington, W. W., and G. A. Meehl, General circulation model CO_2 sensitivity experiments: Snow-sea ice albedo parameterizations and globally averaged surface air temperature, *Clim. Change*, *8*, 231–241, 1986.

Weatherly, J. W., B. P. Briegleb, W. G. Large, and J. A. Maslanik, Sea ice and polar climate in the NCAR CSM, *J. Clim.*, *11*, 1472–1486, 1998.

T. C. Grenfell, P. V. Hobbs, and B. Light, Department of Atmospheric Sciences, University of Washington, Seattle, WA 98195, USA. (tcg@atmos.washington.edu; phobbs@atmos.washington.edu; bonnie@atmos.washington.edu)

D. K. Perovich, Engineer Research and Development Center—CRREL, 72 Lyme Road, Hanover, NH 03755, USA. (perovich@crrel.usace.army.mil)